

Young stars in the periphery of the Large Magellanic Cloud

C. Moni Bidin,^{1*} D. I. Casetti-Dinescu,² T. M. Girard,³ L. Zhang,^{4,5}
R. A. Méndez,⁶ K. Vieira,⁷ V. I. Korchagin,⁸ W. F. van Altena⁹

¹*Instituto de Astronomía, Universidad Católica del Norte, Av. Angamos 0610, Antofagasta, Chile*

²*Department of Physics, Southern Connecticut State University, 501 Crescent Street, New Haven, CT 06515, USA*

³*14 Dunn Rd, Hamden, CT 06518, USA*

⁴*CAS South America Center for Astronomy, Camino El observatorio 1515, Las Condes, Santiago, Chile*

⁵*Key Lab of Optical Astronomy, National Astronomical Observatories, CAS, 20A Datun Road, Chaoyang District, 100012 Beijing, China*

⁶*Departamento de Astronomía, Universidad de Chile, Casilla 36-D, Santiago, Chile*

⁷*Centro de Investigaciones de Astronomía, Apartado Postal 264, Mérida 5101-A, Venezuela*

⁸*Institute of Physics, Southern Federal University, Stachki Street 124, 344090, Rostov-on-Don, Russia*

⁹*Astronomy Department, Yale University, P.O. Box 208101, New Haven, CT 06520-8101, USA*

Accepted XXX. Received YYY; in original form ZZZ

ABSTRACT

Despite their close proximity, the complex interplay between the two Magellanic Clouds, the Milky Way, and the resulting tidal features, is still poorly understood. Recent studies have shown that the Large Magellanic Cloud (LMC) has a very extended disk strikingly perturbed in its outskirts. We search for recent star formation in the far outskirts of the LMC, out to $\sim 30^\circ$ from its center. We have collected intermediate-resolution spectra of thirty-one young star candidates in the periphery of the LMC and measured their radial velocity, stellar parameters, distance and age. Our measurements confirm membership to the LMC of six targets, for which the radial velocity and distance values match well those of the Cloud. These objects are all young (10–50 Myr), main-sequence stars projected between 7° and 13° from the center of the parent galaxy. We compare the velocities of our stars with those of a disk model, and find that our stars have low to moderate velocity differences with the disk model predictions, indicating that they were formed *in situ*. Our study demonstrates that recent star formation occurred in the far periphery of the LMC, where thus far only old objects were known. The spatial configuration of these newly-formed stars appears ring-like with a radius of 12 kpc, and a displacement of 2.6 kpc from the LMC’s center. This structure, if real, would be suggestive of a star-formation episode triggered by an off-center collision between the Small Magellanic Cloud and the LMC’s disk.

Key words: stars: early-type – Magellanic Clouds

1 INTRODUCTION

The Large and Small Magellanic Clouds (LMC and SMC, respectively) form a binary pair of gas-rich, star-forming galaxies that are satellites of the Milky Way, located within ~ 50 kpc of their host. This is a configuration that is rarely found around Milky-Way type galaxies (James & Ivory 2011; Liu et al. 2011). Interactions between the Clouds themselves and with the Galaxy have generated a complex ensemble of gaseous structures such as: the extended Magellanic Stream (Mathewson et al. 1974), encompassing $\sim 200^\circ$ across the sky along the Clouds’ orbit (Nidever et al. 2010); the Bridge between the Clouds (Kerr 1957; Hindman et al.

1963); and the Leading Arm (LA), a fragmented, wide feature leading the orbit of the Clouds (Gardiner & Noguchi 1996, see their Fig. 5). Observational data on the gas in this system have accumulated over the past decades and it is now realized that the Magellanic Stream, Bridge and LA bring to the halo of the Milky Way a mass of gas on the order of $2 \times 10^9 M_\odot$, or over twice as much gas as the Clouds themselves contain (see review by D’Onghia & Fox 2015). Are there any stars in these gaseous features? Tidal models predict the existence of stars, however observations have not been decisive primarily due to the lack of deep, wide and contiguous photometric surveys. While young, recently-formed stars have been found in the Bridge (Irwin et al. 1990; Demers & Battinelli 1998; Harris 2007; Casetti-Dinescu et al. 2012; Skowron et al. 2016) and, more recently, in the LA (Casetti-Dinescu et al. 2014), a sub-

* E-mail: cmoni@ucn.cl

stantial, intermediate-age population is still elusive, with some hints of its presence in the Bridge (Bagheri et al. 2013; Saha & Olszewski 2015; Noël et al. 2015). This status is however improving, primarily due to the Dark Energy Survey (DES), which has recently revealed a large, complex stellar extent to the LMC (Mackey et al. 2016; Belokurov & Koposov 2016) as well as new dwarf galaxies, some of which may be associated with the Magellanic system (see review by D’Onghia & Fox 2015).

In this contribution, we focus on the outskirts of the LMC. Earlier studies based on near-IR surveys agree that the LMC disk extends to some 9 kpc in radius (or about 8° on the sky), and is made of an intermediate to old stellar population. However, Muñoz et al. (2006) report the finding of a handful of giant stars, likely members of the LMC, in the field of Carina dwarf galaxy some 20° away from the LMC’s center. This finding was later confirmed by McMonigal et al. (2014). Saha et al. (2010) present a photometric study in a series of fields that probes the outer regions of the LMC. In particular, the northward fields from a distance of 7° to 20° from the LMC’s center show an exponential decline in the number of stars; this indicates that the intermediate-age/old disk extends out to 16° from the LMC’s center (see Saha et al. 2010, and references therein). Finally, the recent study by Mackey et al. (2016) finds in the same northern region of the LMC a 10-kpc tidal arm at some 16° from the LMC’s center. Clearly the disk of the LMC is very extended and perturbed in its outer parts.

Given that the disk extends so far out, and that it shows evidence of tidal interaction in its outskirts, we seek to know just how far from LMC’s center star formation can occur. This will help us better understand star formation in an environment that was subject to a recent (~ 200 Myr) interaction with the SMC, i.e., a turbulent and tidally stressed environment. To this end, we search for young, newly-formed stars that are LMC members. Casetti-Dinescu et al. (2012, hereafter CD12) listed 567 OB star candidates in a wide area including the periphery of the Clouds, the Bridge, the Leading Arm, and part of the Magellanic Stream. These stars were selected from cuts in magnitude, colors, and proper motions, after merging the UV photometry from the Galaxy Evolution Explorer (GALEX; Bianchi et al. 2011), the infrared data of the Two Micron All-Sky Survey (2MASS; Skrutskie et al. 2006), the optical photometry of the AAVSO Photometric All-Sky Survey (APASS; Henden et al. 2011), and proper motions and photometry from the Southern Proper Motion program (SPM4; Girard et al. 2011). The selection criteria were adjusted to isolate distant, hot, young main-sequence (MS) stars. However, hot subdwarf stars (sdB’s, Heber 1986), and white dwarfs (WDs) should inevitably be present in the sample, because they are photometrically indistinguishable from hot MS stars. These objects are intrinsically fainter than MS stars by more than five magnitudes, hence any such star in the sample will be a foreground Galactic object. Galactic runaway stars could also contaminate the sample to a lesser extent.

We started an extensive spectroscopic campaign to investigate the CD12 young star candidates in more detail (Moni Bidin et al. 2015). In Casetti-Dinescu et al. (2014), we identified some 19 young OB stars in the direction of the LA, where no stellar component was previously known; five of these have kinematics consistent with LA member-

ship and are located at the edge of the Galactic disk. This discovery suggests that the interaction between the Clouds and our Galaxy is strong enough to trigger recent star formation in certain regions of this gaseous structure. However, our analysis also revealed that a relevant fraction (55%) of the candidate sample consists of foreground, more compact Galactic objects. In this paper, we focus on the young star candidates found in the periphery of the LMC, i.e. out to a projected radius of about 33° from the LMC center, while excluding the inner 6° .

2 OBSERVATIONS AND MEASUREMENTS

2.1 Observations and data reduction

We selected thirty-one young star candidates with $V < 16$ between 6° and 33° from the center of the LMC, from the catalog of Casetti-Dinescu et al. (2012). The IDs, coordinates, and V magnitudes of target stars, drawn from the SPM4 catalog (Girard et al. 2011), are given in the first four columns of Table 1. Their intermediate-resolution spectra ($R \approx 3500$) were collected during three half-nights of observations between 2015 January 28 and February 22 at Las Campanas Observatory, with the IMACS spectrograph at the focus of the Baade 6.5m telescope. The instrument was used at $f/4$ in longslit mode, and the $0''.75$ -wide slit was employed. The 1200–17.5 grating was tilted by an angle of 16.8° to cover the spectral range 3660–5250 Å on the CCD. Exposure times varied between 150s and 1500s, according to target magnitude and sky conditions, to yield spectra with signal-to-noise ratio $S/N > 50$. A comparison lamp for wavelength calibration was acquired after each exposure. A twilight solar spectrum was collected at the beginning of each night, and the radial-velocity standards LTT2415 (Latham et al. 2002) and GJ273 (Chubak et al. 2012) were also observed.

The spectra were split on four chips with short gaps between them. Each spectral section was independently reduced, extracted with an optimum algorithm (Horne 1986) and normalized, with standard IRAF¹ routines (see, e.g., de la Fuente Marcos et al. 2015). Before merging them, the absolute offsets of the four independent wavelength calibration solutions were measured on the standard stars, and corrected. Some reduced spectra are shown in Fig. 1 as an example.

2.2 Radial velocities

We measured the radial velocity (RV) of target stars using IRAF task *fxcor*, cross-correlating (Simkin 1974; Tonry & Davis 1979) their spectra with synthetic templates drawn from the library of Munari et al. (2005). Previous investigations have shown that the RV measurements are not affected by the exact choice of the template, because a partial mismatch between object and template spectral types only enhances the formal uncertainties, without shifting the peak of the cross-correlation function (Morse et al.

¹ IRAF is distributed by the National Optical Astronomy Observatories, which are operated by the Association of Universities for Research in Astronomy, Inc., under cooperative agreement with the National Science Foundation.

Table 1. Data and measurements of target stars.

SPM ID	RA h:mm:ss.s	Dec °:':"	V	RV km s ⁻¹	T_{eff} K	$\log(g)$ dex	$\log(\frac{N(\text{He})}{N(\text{H})})$ dex	$V \sin(i)$ km s ⁻¹	note
0030025059	3:32:14.6	-83:44:13	14.08	183±6	17000±250	3.88±0.06	-1.00	< 50	MS
0870012815	3:42:24.1	-64:03:21	14.82	19±7	18800±350	4.69±0.06	-2.20±0.09	~ 50	sdB/WD
0140123632	3:47:26.8	-78:41:54	15.90	413±11	15900±500	3.81±0.09	-2.15±0.15	~ 50	post-HB?
0570014281	3:50:37.7	-69:20:57	14.70	-24±15	42600±200	6.19±0.09	+0.15±0.09	~ 50	sdB/WD
0320149401	4:13:50.7	-72:18:52	15.95	26±10	25300±500	5.55±0.06	-2.83±0.12	< 50	sdB/WD
0320022407	4:15:21.2	-72:51:41	13.93	-4±7	24100±500	5.18±0.06	-2.56±0.12	< 50	sdB/WD
1660012832	4:15:30.2	-54:21:59	14.91	-7±21	50600±700	6.50±0.09	+0.34±0.27	< 50	sdB/WD
0880011003	4:19:30.8	-65:22:13	13.98	12±6	25300±500	5.02±0.06	-2.08±0.09	< 50	sdB/WD
0320115607	4:19:55.5	-73:51:45	16.04	164±9	24500±400	4.03±0.06	-1.03±0.09	~ 100	MS
0320018938	4:19:58.5	-73:52:26	14.95	193±8	22300±400	3.78±0.09	-1.02±0.09	~ 100	MS
0040202213	4:20:32.1	-82:06:35	15.89	-27±21	47500±800	6.14±0.15	+0.78±0.18	< 50	sdB/WD
1250013582	4:26:29.2	-59:06:10	14.29	-17±6	26000±500	5.41±0.06	-2.84±0.09	< 50	sdB/WD
1250015381	4:36:09.8	-58:37:07	14.90	212±7	21100±400	3.50±0.09	-0.95±0.09	~ 100	MS
2740050272	4:42:20.2	-45:52:29	15.73	50±12	59000±3000	6.01±0.12	-2.22±0.15	< 50	sdB/WD
1270012151	5:16:10.6	-60:57:37	14.81	2±6	25700±400	5.40±0.06	-2.66±0.09	< 50	sdB/WD
1680007950	5:29:01.2	-56:33:10	15.06	43±7	27400±400	5.50±0.06	-2.53±0.09	< 50	sdB/WD
0340108821	5:57:02.2	-75:40:23	16.04	-52±11	-	-	-	-	sdB/WD
1280025746	5:58:49.6	-58:56:27	15.25	303±5	21700±350	3.65±0.06	-1.00	< 50	MS
1280143250	6:00:00.6	-59:01:03	16.01	-34±9	42200±300	5.62±0.15	+0.58±0.09	< 50	sdB/WD
1280031295	6:00:22.1	-57:54:20	15.54	368±8	16000±250	3.33±0.06	-1.00	~ 50	MS
0910042645	6:05:34.6	-62:55:06	15.66	-12±7	27800±400	5.48±0.06	-2.89±0.12	< 50	sdB/WD
3380011095	6:15:47.1	-41:32:06	14.65	424±6	16100±200	4.05±0.06	-1.00	< 50	MS
1280035162	6:20:38.5	-57:05:38	14.72	-11±5	34100±500	5.60±0.06	-0.89±0.06	< 50	sdB/WD
0350036197	6:46:44.1	-72:10:37	13.64	23±5	29400±900	5.14±0.12	-1.16±0.09	< 50	sdB/WD
0600320649	6:48:41.5	-68:30:36	16.14	-4±16	42400±300	5.66±0.15	+0.55±0.09	< 50	sdB/WD
0600047219	6:53:13.1	-66:59:51	14.64	55±9	37500±900	5.38±0.12	-3.16±0.18	< 50	sdB/WD
0920126094	6:59:58.0	-66:18:28	16.38	284±7	19100±400	3.78±0.06	-1.00	~ 100	MS
0350232289	7:04:25.2	-72:38:43	15.89	280±8	22400±600	3.69±0.09	-1.00	~ 200	MS
0350031043	7:10:55.1	-73:27:21	15.18	-35±7	27100±600	5.39±0.09	-2.64±0.12	< 50	sdB/WD
1310017952	7:48:37.5	-61:50:03	14.91	8±6	27000±500	5.45±0.06	-2.18±0.09	< 50	sdB/WD
0950048906	8:39:21.8	-64:49:35	15.55	27±8	32900±400	5.46±0.06	-3.33±0.12	< 50	sdB/WD

1991; Moni Bidin et al. 2011). All RVs were corrected to heliocentric values. The results are given in the fifth column of Table 1. The errors were computed as the quadratic sum of the most relevant sources. The wavelength calibration introduced a negligible uncertainty, smaller than 1 km s⁻¹ for all stars. The cross-correlation error was in the range 2–8 km s⁻¹ (but up to 15–20 km s⁻¹ in four cases), and thus it usually dominated the error budget. Some systematic offsets are expected, caused by an imperfectly-centered position of the star in the slit (see the discussion in Moni Bidin et al. 2006). These are hard to estimate and remove, in absence of deep telluric lines in the observed spectral range. Instead, they were estimated from the rms of the residual RV offsets of the standard stars, and thus approximated as a fixed 4 km s⁻¹ for all targets. The spectra were eventually shifted to laboratory wavelength for the measurement of the stellar parameters.

2.3 Stellar parameters

The temperature, gravity, and surface helium abundance of the target stars were measured by fitting the observed hydrogen and helium lines with synthetic spectra. The model spectra were computed with Lemke’s version² of the

Linfor program (developed originally by Holweger, Steffen and Steenbock at Kiel University), fed with model atmospheres computed with ATLAS9 (Kurucz 1993). The metallicity was set to solar, as appropriate for both recently-formed stars and hot foreground subdwarfs, whose atmospheres are enriched with heavy elements due to diffusion processes (Moehler et al. 2000). The grid of templates covered the range $8\,000 \leq T_{\text{eff}} \text{ (K)} \leq 35\,000$, $2.5 \leq \log(g) \leq 6.0$, $-3.0 \leq \log(\frac{N(\text{He})}{N(\text{H})}) \leq -1.0$. The synthetic spectra were convolved with a Gaussian during the fitting procedure, to match the instrumental resolution of the data. The spectra of the few evolved objects hotter than 35 000 K were fitted using a grid of metal-free non-LTE models described in Moehler et al. (2004), calculated as in Napiwotzki (1997).

The best fit and the derivation of the stellar parameters were established through the routines developed by Bergeron et al. (1992) and Saffer et al. (1994), as modified by Napiwotzki et al. (1999). The code normalizes both the model and the observed spectra simultaneously using the same points for the continuum definition, and makes use of a χ^2 test to establish the best fit. The noise in the continuum spectral regions is used to estimate the σ for the calculation of the χ^2 statistics, which the routines use to estimate the errors of the parameters (see Moehler et al. 1999). However, they thus neglect other sources of errors, such as those introduced by the normalization procedure, the sky subtraction,

² <http://a400.sternwarte.uni-erlangen.de/~ai26/linfit/linfor.html>

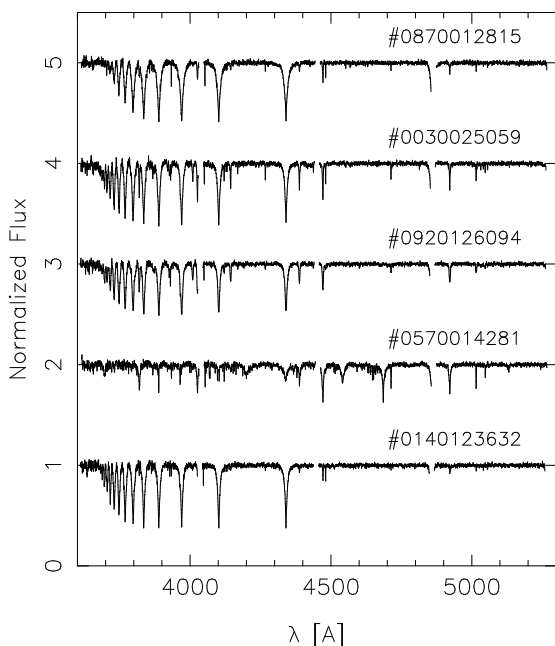


Figure 1. Examples of reduced spectra of our sample stars. The spectra are shifted vertically to avoid overlap. The SPM ID of each target is also indicated. From top to bottom, we show the spectrum of a helium-poor sdB, a MS star at the same temperature, a fast-rotating MS object, a hot WD, and the uncertain SPM4 object 0140123632 discussed in Sect. 3.1.

and the flat-fielding. Therefore, the resulting uncertainties were multiplied by three to obtain a more realistic estimate of the true errors (Napiwotzki 2005, priv. comm.). The lines of the Balmer series from H_β to H_{12} were simultaneously fitted, along with four He I lines (4026 Å, 4388 Å, 4471 Å, 4922 Å). Two He II lines (4542 Å, 4686 Å) were also included when visible in the spectra of hot stars. Results for all the targets are given in Table 1. We could not find a good solution for the spectrum of star SPM4 0340108821, nor could we determine if this was due to problems related to its spectrum, or to limitations of our model grid. This object will therefore be excluded from further analysis. However, its strong and wide He II lines reveal that it is most likely a foreground WD ($\log(g) > 6$, $T_{\text{eff}} > 40000$ K).

The lines of some stars were clearly broadened due to high projected rotational velocity. The employed routine did not include $V \sin(i)$ as a fit parameter, but as a fixed input quantity beforehand. We then estimated $V \sin(i)$ varying this value manually in such a way as to minimize the resulting χ^2 of the fit. A precise estimate of $V \sin(i)$ is not possible due to the relatively low resolution. In addition, the wide Balmer lines dominated the fit statistics, but these features were intrinsically too wide for this purpose. As a consequence, our results are reliable only for a rough distinction between stars showing no relevant evidence of rotation ($V \sin(i) < 50$ km s $^{-1}$), stars showing hints of rotation ($V \sin(i) \sim 50$ km s $^{-1}$), and fast rotators ($V \sin(i) \sim 100$ or 200 km s $^{-1}$). The results are given in the ninth column of Table 1.

The surface helium abundance was assumed as a fit parameter in the procedure, and the model grid spanned a wide range from solar value ($\log(\frac{N(\text{He})}{N(\text{H})}) = -1$) down to one-

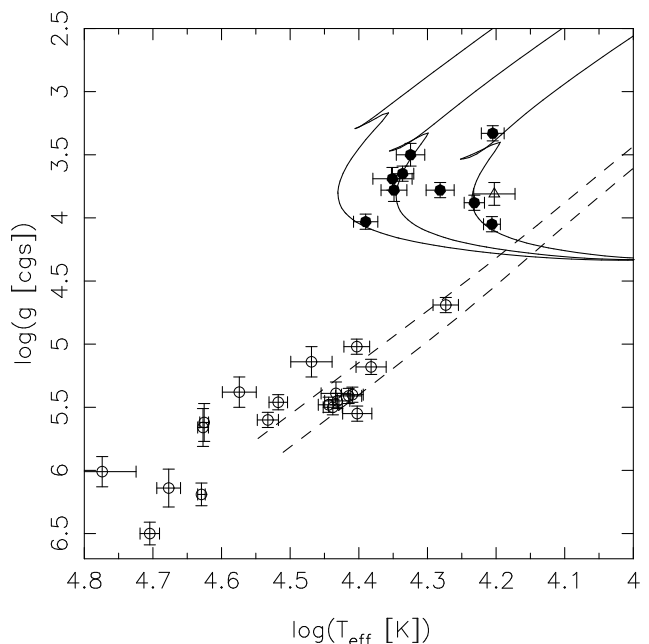


Figure 2. Location of the program stars in the temperature-gravity plane. Filled and open circles represent MS and foreground compact objects, respectively. The open triangle indicates the star whose classification is uncertain. Solid curves show solar-metallicity isochrones of 10, 20, and 50 Myr. The dashed curves indicate the zero-age and terminal-age horizontal branch.

thousandth of solar abundance. This is appropriate for foreground subdwarfs, and this is, in fact, a key parameter to identify them in our sample (see Sect. 3.1). However, diffusion processes are not active in MS stars, and their surface helium abundance is in general close to solar. This parameter is therefore not very informative for these objects. On the other hand, we found that fixing $\log(\frac{N(\text{He})}{N(\text{H})}) = -1$ led to better fits of all the lines for some MS stars. We adopted the results obtained with helium abundance fixed to solar for these objects, and this parameter has no associated error in Table 1. We nevertheless verified that our final results were not affected by this choice as, for example, distance moduli and ages changed by less than $1-1.5\sigma$.

3 RESULTS

3.1 MS stars and foreground objects

The RV distribution of target stars is clearly bimodal, with a huge gap between ten high-velocity stars ($RV > 160$ km s $^{-1}$) and the rest of the sample ($RV < 55$ km s $^{-1}$). This dichotomy suggests an easy separation between LMC members and foreground stars, because the RV of the LMC (262.1 ± 3.4 km s $^{-1}$ van der Marel et al. 2002) is very high compared to the typical RV of Galactic stars along the same line of sight. However, our single-epoch measurements alone are not enough to uniquely identify LMC stars from Galactic interlopers, since the incidence of close binaries is very high among both massive OB stars (Sana et al. 2012) and subdwarfs (Maxted et al. 2001), although the binary fraction for old halo sdB's could be much lower than in the disk (Moni Bidin et al. 2008; Han 2008). Galactic run-

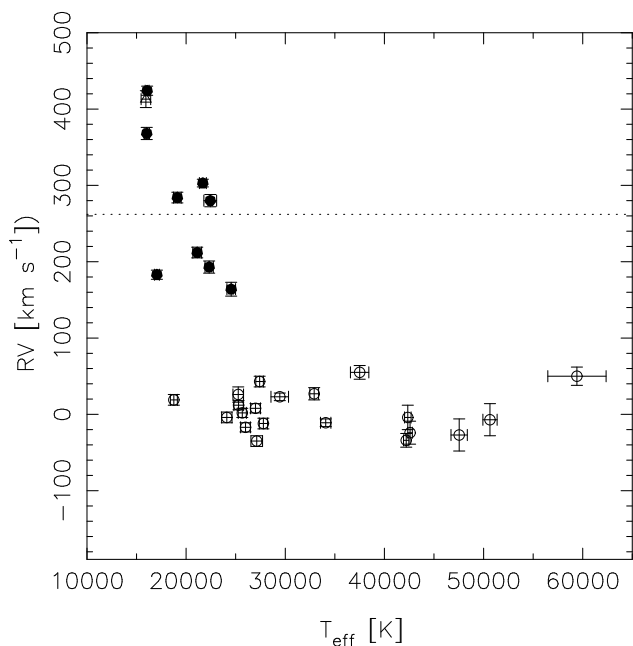


Figure 3. RV of target stars as a function of their effective temperature. The symbols are as in Fig. 2. The dotted line indicates the systemic RV of the LMC.

away stars, on the other hand, are predominantly single objects (Mason et al. 1998), but they can show anomalously high RV due to their intrinsic nature of being high-velocity stars. However, the measured stellar parameters provide a straightforward identification of sdB’s and WDs. In fact, their surface gravity is higher than that of MS stars at the same temperature for $T_{\text{eff}} > 15000$ K (see, e.g., Salgado et al. 2013), and their loci in temperature-gravity space are well separated. The atmospheres of sdB’s with $T_{\text{eff}} < 35000$ K are also depleted of helium (typically $\log(\frac{N(\text{He})}{N(\text{H})}) < -1.5$, Moni Bidin et al. 2009), at variance with the close-to-solar values expected for MS stars. In addition, while fast rotators are common in the MS, they are extremely rare among sdB’s (Geier & Heber 2012).

Figure 2 shows the position of target stars in the temperature-gravity plane. Solar-metallicity isochrones from Bressan et al. (2012) are also shown as solid curves. Dashed lines indicate the zero-age and terminal-age horizontal branch, which enclose the loci where stars spend 90% of their helium core-burning stage. Twenty stars lie on the loci of sdB’s and WDs, and their surface gravity is too high for MS objects ($\log(g) > 4.7$). All but two of the high-gravity stars with $T_{\text{eff}} < 40000$ K are strongly helium-depleted $\log(\frac{N(\text{He})}{N(\text{H})}) < -2$, while surface helium abundance increases for the hottest stars up to super-solar values, as is usual for O-type subdwarfs and hot WDs (e.g., Edelman et al. 2003). Only two of these stars show hints of rotation (SPM4 0870012815 and SPM4 0570014281). All these objects are therefore classified as foreground stars. The gravity of the coolest star of our sample (SPM4 0140123632) is too low to be an sdB. However, its very low helium abundance is incompatible with it being an MS star. While its classification should be regarded as dubious, we interpret it as a post-horizontal branch star, evolving at lower gravities toward the Asymptotic Giant Branch after exhaustion of helium in the core. It should

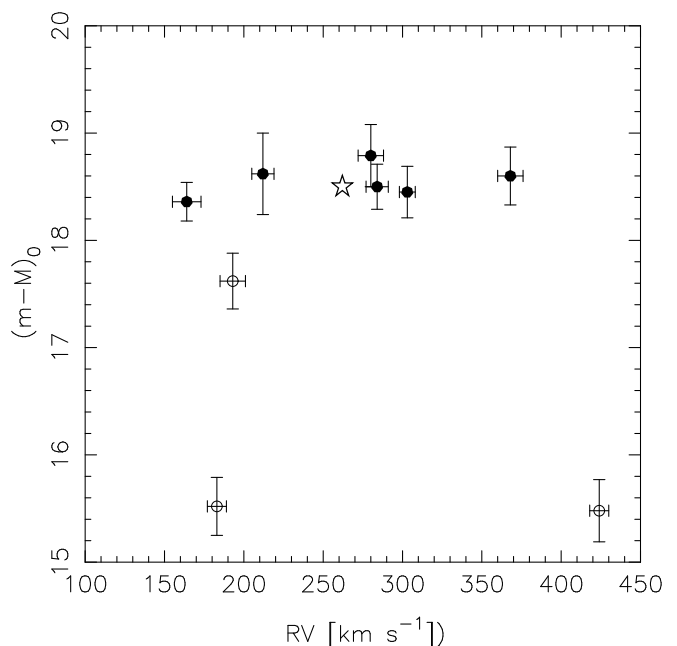


Figure 4. Distance modulus of the target MS stars as a function of their RV. Filled and open circles indicate the LMC members and the foreground runaway stars, respectively. The star symbol indicates the value of the LMC.

be a foreground object even in this case, because its absolute magnitude would have to be too bright for a post-HB star at its temperature to place it at the distance of the LMC ($(m-M)_0 \approx 18.5$, Freedman et al. 2001). The remaining nine targets are clearly MS stars, as deduced from their position in the temperature-gravity plane and their close-to-solar surface helium abundance. Six of them also show evidence of non-negligible rotation. The classification of each target (“sdB/WD”, “post-HB?”, or “MS”) is given in the last column of Table 1.

The RVs of our targets are shown in Fig. 3 as a function of effective temperature, where we indicate foreground compact objects and MS stars with empty and full symbols, respectively. The Figure reveals that the RV of all foreground sdB’s/WDs is lower than 55 km s^{-1} , while the aforementioned high-velocity stars are all MS stars, with the addition of the uncertain post-HB object. The foreground stars will not be considered further, and we will focus on the nine MS stars hereafter.

3.2 Distances and ages

The age of the MS stars was estimated comparing their position in the temperature-gravity plane with solar-metallicity isochrones, as shown in Fig. 2. Varying the stellar parameters within their error bars caused small variations in the derived age, of the order of 10%. A larger uncertainty was introduced by the assumption of the isochrone metallicity, as a change of ± 0.5 dex affected the results by $\mp 20\%$ or more. We therefore assumed this uncertainty as the final error.

The observed V magnitudes were de-reddened by means of the line-of-sight values given by the Schlegel et al. (1998) maps, as corrected by Bonifacio et al. (2000), assuming a standard reddening law ($R = \frac{A_V}{E(B-V)} = 3.1$). An estimate of the

Table 2. Reddening, age, distance modulus, V_{lsr} and Magellanic coordinates of the target MS stars.

ID	SPM ID	$E(B-V)$ mag	age Myr	$(m-M)_0$ mag	V_{lsr} km s $^{-1}$	ξ_{Λ_M} °	η_{B_M} °
005	0030025059	0.10	50±20	15.52±0.27	174	-2.281	-12.611
292	0320115607	0.10	11±6	18.36±0.18	153	-4.247	-2.510
290	0320018938	0.10	20±5	17.62±0.26	182	-4.240	-2.519
403	1250015381	0.01	20±5	18.62±0.38	198	-7.065	12.871
405	1280025746	0.04	20±5	18.45±0.24	288	3.910	13.412
406	1280031295	0.05	45±10	18.60±0.27	353	4.220	14.491
487	3380011095	0.07	55±30	15.48±0.29	407	9.457	33.541
390	0920126094	0.11	35±8	18.50±0.21	271	9.310	4.555
307	0350232289	0.16	18±5	18.79±0.29	268	7.447	-1.609

distance modulus was thus obtained, by comparison with the absolute magnitude in the V band obtained from the same solar-metallicity isochrones. The assumption of $[\text{Fe}/\text{H}] = \pm 0.5$ for the theoretical isochrones shifted the absolute magnitude by ∓ 0.2 mag at most (∓ 0.12 mag on average). A larger but comparable uncertainty on $(m-M)_0$ was induced by the observational errors of the stellar parameters (0.23 mag on average), and the two values were quadratically summed to obtain the final errors. The results for reddening, age, distance modulus, and line-of-sight velocity with respect to the Local Standard of Rest V_{lsr} are given in Table 2, where we also add an internal ID (first column) and sky coordinates (see Section 4).

Figure 4 shows the RV of our MS objects as a function of their distance modulus, compared to the LMC values $RV_{\text{LMC}} = 262.1 \pm 3.4$ km s $^{-1}$ (van der Marel et al. 2002) and $(m-M)_{0,\text{LMC}} = 18.5$ (distance $d = 50$ kpc; Freedman et al. 2001). Two stars are clearly foreground objects ($(m-M)_0 \approx 15.5$, $d \approx 12.5$ kpc). A third more distant star ($d \approx 33$ kpc), whose $(m-M)_0$ is incompatible with the LMC at the 3.3σ level, is also likely not a LMC member. These three stars are probably Galactic runaway stars, as also suggested by their high recession velocity. The distance modulus of the six remaining stars agrees with the LMC value within 1σ . Therefore, we consider these six young stars as being members of the LMC.

4 ANALYSIS

In what follows, we adopt the Magellanic coordinate system introduced by Nidever et al. (2010), in which Λ_M is the longitude along the Magellanic Stream, positive toward the direction of motion of the LMC (i.e., toward the Galactic plane), and B_M is the Magellanic latitude. Our adopted center for the LMC is (RA, Dec) = (81° 90, -69° 86), from van der Marel et al. (2002). This center, however, does not correspond to the origin of the Magellanic coordinate system, but is slightly offset: $(\Lambda_{M,\text{LMC}}, B_{M,\text{LMC}}) = (0^\circ 215, 2^\circ 330)$. We adopt this system since it reflects the orbital motion of the LMC, and — at the location of the LMC — it is closely aligned with the equatorial system (a $\sim 2^\circ$ offset). Finally, the spherical (Λ_M, B_M) coordinates are projected onto a plane tangent to the sky at $(\Lambda_M, B_M) = (0^\circ, 0^\circ)$, a gnomonic projection with coordinates $(\xi_{\Lambda_M}, \eta_{B_M})$. Units for sky coordinates are degrees throughout the paper.

4.1 Matching with Existing Catalogs of Clusters and Associations

We have cross-matched our six stars with the catalogs of Bica et al. (2008). In Fig. 5 we show the spatial distribution of our six stars, and of the catalog of clusters (left panel), young associations (middle panel) and emission nebulae (right panel). Target #403 is 15' from the center of the globular cluster Reticulum. However, this star is not a cluster member, since it is a young star, and its RV of 212 ± 7 km s $^{-1}$ is different from that of the cluster (241.5 ± 1.5 km s $^{-1}$ Suntzeff et al. 1992). In Fig. 5, we also mark the newly-found, loose cluster by Piatti (2016). This 280 Myr open cluster is at a distance some 11.3 kpc larger than that of the LMC. However, its sky location is well within the distribution of the clusters catalogued by Bica et al. (2008).

The target #292 is within the stellar association ICA76 (aka IDK6) as given in Bica et al. (2008), Irwin et al. (1990), and Battinelli & Demers (1992). Specifically, #292 is at 2' from the center of ICA76, which has a radius of $\sim 7'$ (Bica et al. 2008). We note that star #290 is also located within the projected radius of ICA76, but the distance modulus determined here (Tab.2) places it in the foreground. Demers & Battinelli (1998) determine a distance modulus of 18.63 ± 0.10 to ICA76, and an age of 10-25 Myr. This agrees reasonably well with the distance and age of star #292 (see Tab.2). Demers & Battinelli (1998) also quote previous RV measurements of these two stars: they are 194 km s $^{-1}$ and 270 km s $^{-1}$ for #290 and #292, respectively. Their RV for #290 agrees with our measurement (193 ± 8 km s $^{-1}$), however that for #292 does not (164 ± 4 km s $^{-1}$). While we don't have an explanation for this discrepancy, one reason may be binarity.

We have cross-matched our six stars with the recent DES cluster catalog by Pieres et al. (2016), and found no matches. We have also inspected $15' \times 15'$ GALEX and Digital Sky Survey B images centered on each of our six stars. Excepting #292, where the stellar association ICA76 is clearly visible, the remaining five stars appear isolated. To conclude, our six young stars are much further out in projected distance from the LMC's center than the catalogued clusters, associations, and emission nebulae. Only one star in our sample is a likely member of a known young stellar association located in the Bridge, while the other five objects cannot be identified as being associated with any known stellar aggregate.

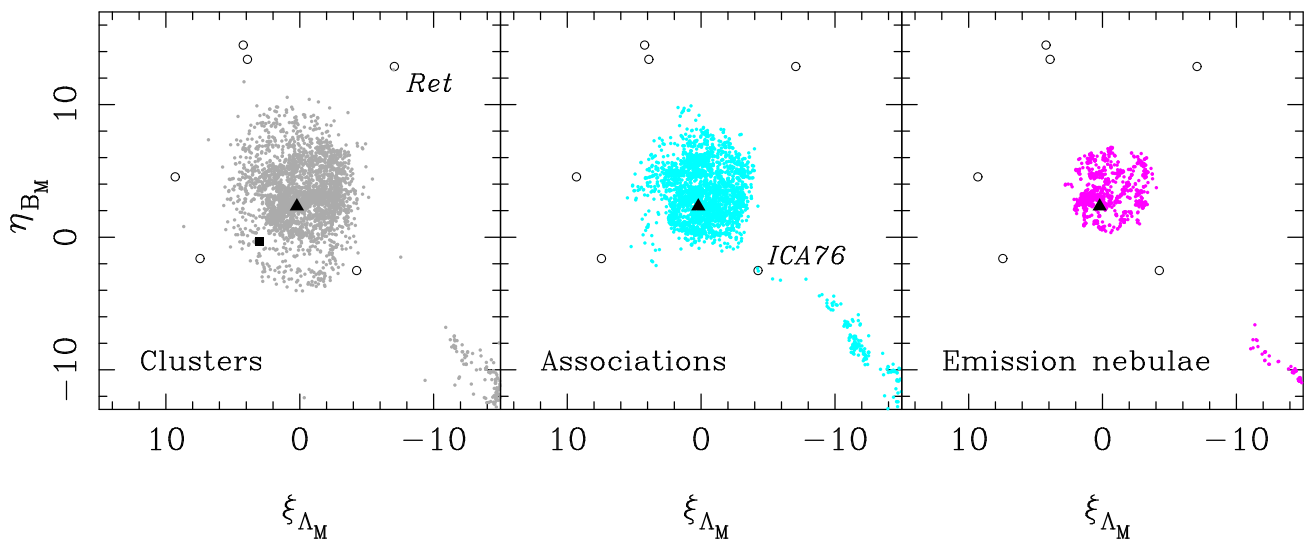


Figure 5. Spatial distribution of our six young stars (open circles) compared to that of clusters (left), young associations (middle), and emission nebulae (right) from Bica et al. (2008). The center of the LMC is marked with a triangle. The positions of the globular cluster Reticulum and the stellar association ICA76 are also labeled. The dark square marks the newly-discovered, loose cluster by Piatti (2016).

4.2 Spatial Distribution

In Figure 6 we show the area coverage of the CD12 study to select OB-type candidates in the region of the Clouds. Gaps in the coverage are primarily due to the GALEX GR5 survey. Candidates from CD12 are shown with crosses: clearly, only the outer regions of the Clouds were probed by CD12. The Galactic plane is toward the left of this Figure. We also mark two useful locations in this plot: the center of Carina dwarf galaxy, and the first detection of HCO^+ absorption at the leading edge of the Magellanic Bridge by Murray et al. (2015). Muñoz et al. (2006) found giant stars, likely members of the LMC in the Carina foreground, thus hinting at the large spatial extent of the Cloud, while the detection of HCO^+ is indicative of star formation. Figure 6 is meant to caution the reader as to the areal incompleteness.

In Fig. 7 we show the map of the H I column density in our region centered on the LMC. The H I data are from the GASS III cleaned data described in Kalberla & Haud (2015), within the velocity range $V_{lsr}=100$ to 450 km s^{-1} . OB-type candidates from CD12 are shown with grey crosses. Stars observed spectroscopically in this study are shown with circles, young stars being highlighted in green, and the six LMC members are marked with a square. As in Fig. 6, Carina’s center and the location of HCO^+ detection are indicated. The thick blue line marks the newly found 10-kpc tidal feature/arm by Mackey et al. (2016) in the DES. The thick blue dotted line marks the western extension of this arm, a feature less conspicuous than the arm.

Our six stars are surrounding the LMC out to $\sim 13^\circ$ from its center. Star #292 which belongs to association ICA76 is clearly located in the Bridge, and it is the closest in projected distance to LMC’s center. Two stars, #405 and #406, are very close to each other (within $\sim 1^\circ$), while the remaining three are at various position angles. Except for #292 which is in the Bridge, the stars are in regions of low H I column density, $N_{HI} < 10^{19} \text{ cm}^{-2}$. It is intriguing that the two close together stars, #405 and #406, are only some 5° behind the stellar tidal arm found by Mackey et al. (2016).

Mackey et al. (2016) also indicate the existence of a western extension of this tidal arm in their Fig. 2 (the blue dotted line in our Fig. 7). This extension, if real, is very near to our star #403, with the star slightly closer to the LMC center than the extension. We also note that Besla et al. (2016) found stellar arcs and spiral arms in the northern periphery of the LMC. These features are within $\sim 8^\circ$ of the LMC’s center, specifically in region C of Besla et al. (2016), their Fig. 4. Our study does not properly sample these structures, since we focused on more distant objects (see Fig. 7). None of our candidates lying close to the HCO^+ detection proved to be LMC members, but that region of the sky is affected by a large areal gap in the survey data (see Fig. 6).

4.3 Testing a Ring-like Configuration

Our five stars (excluding the ICA76 member) appear to be in a half-ring configuration, with the ring’s center some 3° northward of LMC’s center, and spanning some $\sim 140^\circ$ in position angle (see Fig. 7). Note that some 10-12 candidates at moderate $\sim 7^\circ - 10^\circ$ distance from the LMC’s center are foreground stars (see open circles in Fig. 7). This leaves a gap between a region of inner star formation, as traced by emission nebulae and young associations (Fig. 5), and the off-center, ring-like configuration of our five stars. Also, the five stars coincide with the “near” part of the LMC disk (see Fig. 9). Alas, our distance uncertainties are inadequate to explore the “nearness” of these five stars.

Our targets were selected from the CD12 candidates located between 6° and 33° from the center. Hence, the spatial distribution of the observed sample has already some degree of circular symmetry about the LMC center. One might wonder to what extent the ringlike feature traced by the five young LMC stars could be an effect induced by the underlying distribution of the selected targets. That is, while the stars found to be young LMC members appear to lie in the form of a ring, are they really that much more “ring-like” than other, random groupings of five stars that might

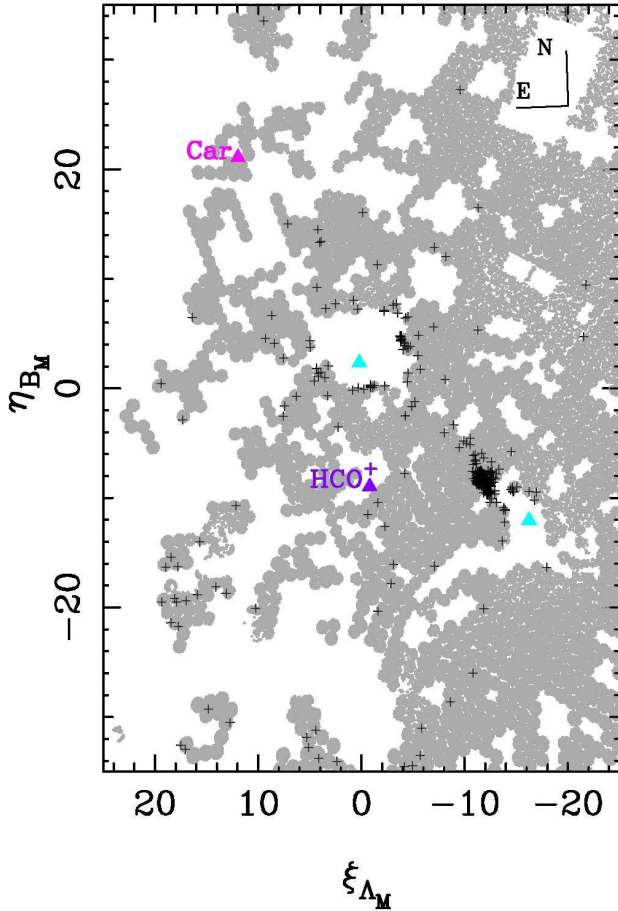


Figure 6. Area coverage of the CD12 study to select candidates (grey background). The round footprint of GALEX is easily visible; the gaps in area coverage are mainly due to the GALEX GR5 coverage. Young, OB-type star candidates from CD12 are shown with crosses. The centers of the LMC and SMC are shown with light-blue triangles. Two notable sky locations are also indicated and labeled: the Carina dwarf galaxy and the first detection of HCO⁺ absorption in the Magellanic System by Murray et al. (2015). North and East directions are also indicated.

have been drawn from the observed sample? To answer this question, we perform a Monte Carlo test to quantify the statistical significance of the observed configuration.

From the 31 spectroscopically observed stars we discard four that are located in the Bridge. From this set of 27 stars, we randomly select five stars and project their sky positions into the LMC disk plane. The geometry of the disk is adopted from Olsen et al. (2011), with an inclination angle of 34.7°, and a position angle of the line of nodes of 142.0° (see also Sec. 4.4). We search in a grid around the LMC’s center for a ring-center position that gives the five stars a minimum in $\delta r/r_{ave}$, where r_{ave} is the average radius of a circle they define, and δr is the root-mean-square scatter of the stars’ positions from a perfect circle. The optimal center and r_{ave} define the “best-fit” circular ring for this group of five stars. We also calculate the arc length that the five stars subtend along the best-fit circle. The search for the ring center is done in steps of 0.25° within 7° of the LMC’s center. We perform 1000 such random, five-star trials and store the resulting values of $\delta r/r_{ave}$ and arc length. Then, we repeat

this 1000-trial run a total of ten times. For each run, we determine how many groups of five stars form a “better” circle than the actual five LMC stars, i.e., have $\delta r/r_{ave}$ smaller than that of the five LMC stars. We find that the angular arc length of our five stars is fairly typical of randomly drawn ones. However, on average, only 1.35% of randomly drawn groups form an arc of a circle with $\delta r/r_{ave}$ lower than that of the five LMC stars. This result suggests that an accidental hypothesis can be ruled out at the 98.65% confidence level. The ringlike configuration of these five stars is therefore unlikely to be due to chance, and a physical basis is suggested. We speculate as to the possible origin of such a structure in Sec. 4.5.

The ring parameters found for the five LMC stars are: average radius $r_{ave} = 13.1^\circ$, distance from the LMC’s center $\rho = 3.0^\circ$, and position angle arlength $\Delta PA = 145^\circ$. At a distance of 50 kpc for the LMC, the average radius is 12 kpc, and the distance from LMC’s center is 2.6 ± 0.3 kpc. All of these parameters are in the LMC’s disk plane.

While our statistical test shows it is unlikely that the ring is mere coincidence – and we proceed to derive the geometry in the plane of the LMC as if this were a real structure – this is all based on five stars situated over a rather large portion of sky. Determining whether these stars actually reside in the LMC disk will require additional observations (primarily astrometric) that are not available at this time.

4.4 Velocity Distribution

We compare our measured radial velocities for the LMC members with that of the H I gas (Kalberla & Haud 2015) in Fig. 8. Plotted is the local standard of rest radial velocity V_{lsr} as a function of ξ_{LM} , the coordinate along the orbit of the LMC. The color scale represents the temperature brightness integrated along η_{BM} for the range -30° to 30° . The location of the Galactic disk, and of the central parts of the Clouds are clearly visible. Our young LMC members are shown with green symbols. They follow the overall pattern of the gas motions, with the two most deviant points being star #292 at $\xi_{LM} = -4.247^\circ$, and star #406 at $\xi_{LM} = 4.220^\circ$. Star #292 is a member of ICA76, located in the Bridge; and in Section 4.1 we noted a previous velocity measurement for this star ($RV = 270 \text{ km s}^{-1}$, or $V_{lsr} = 259 \text{ km s}^{-1}$), which would bring it in better agreement with the gas motion.

We also compare our velocity measurements with the predictions of a disk model for the LMC. We adopt the geometry and rotation curve of the disk from Olsen et al. (2011); these were determined from the analysis of red supergiants, a relatively young population. The adopted distance to the LMC is 50 kpc, and its RV is 263 km s^{-1} . The inclination angle of the disk is 34.7°, and the position angle of the line of nodes is 142.0°. The model assumes circular motions only, and we use the formalism from van der Marel et al. (2002) to calculate velocities at a given position angle and angular distance from the LMC’s center. The arrows in Fig. 8 point to the velocity model predictions at each star’s location in (ξ_{LM}, η_{BM}) , i.e., the length of the arrow is the velocity difference between observation and model. These differences are rather modest, indicating that the velocities of the stars are not too deviant from simple, circular motion in the disk of the LMC.

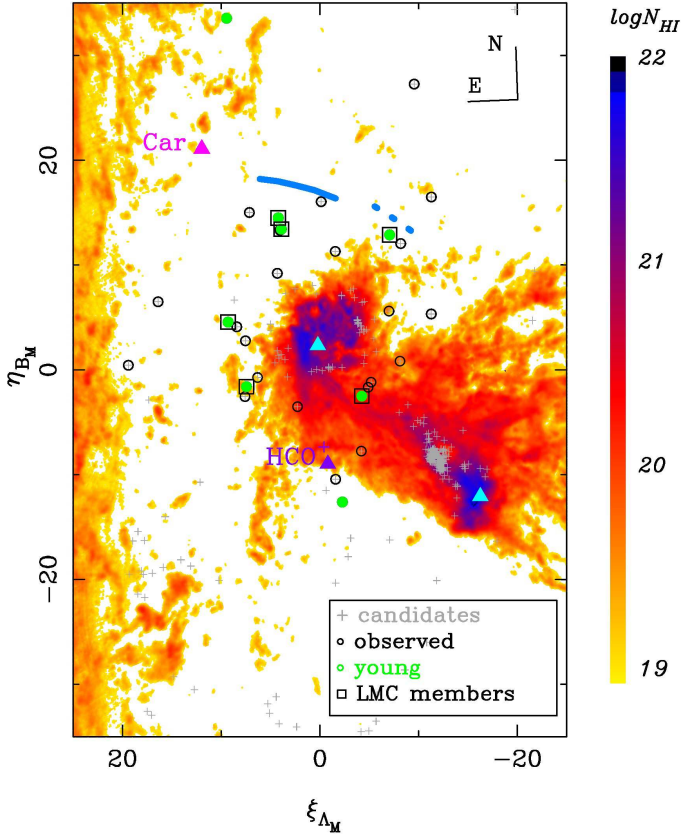


Figure 7. Map of the H I column density from the GASS survey within $V_{lsr}=100$ to 450 km s^{-1} in the region of interest. The centers of the Clouds are shown with light blue triangles. OB-type candidates from CD12 are shown with grey crosses. Circles represent the stars observed spectroscopically in this study. Filled green circles indicate the young stars. Squares indicate the six young stars that are members of the LMC. The thick blue curve indicates the newly found 10-kpc tidal feature/arm by Mackey et al. (2016) in the Dark Energy Survey. The thick dotted blue curve shows the western extension of this arm.

To explore whether the velocity differences have any correlation with distance from LMC center, or with the position angle, we plot these velocity differences at the sky location of each star in Fig. 9. For reference, we show isodensity contours of M giants in the LMC selected from 2MASS as in CD12. The LMC’s bar is easily visible in the inner regions. We also mark the location of the star-forming region 30 Doradus with a green square. The line of nodes of the disk is shown with a dashed line, and the “near” and “far” halves of the disk are labeled. The six young LMC members are shown with circles, and the member of ICA76 is highlighted with a star symbol. A circle with a radius of 15° centered on the LMC is also shown. Velocity differences do not show a correlation with either projected distance from LMC center or with position angle. The average of these differences is -16 ± 15 km s^{-1} , with a standard deviation of 36 km s^{-1} . If we exclude star #292, the member of ICA76, we obtain an average velocity difference of -9 ± 16 km s^{-1} , with a similar standard deviation of 36 km s^{-1} .

4.5 Origin of the Young Stars

Inspecting Table 2, we see that star #292 is 11 Myr old, the youngest in our sample of six stars. The ages of the remaining five stars range between 18 and 45 Myr, with an average of ~ 30 Myr. If we assume the standard deviation of the line-of-sight velocities is representative of the deviations from simple LMC disk rotation for the tangential components as well, we can estimate the maximum distance in the sky these stars will travel in 30 Myr. For 36 km s^{-1} (Section 4.4), this distance amounts to 1 kpc, or $\sim 1^\circ$ at the distance of the LMC. Thus, in absence of precise proper motions for these stars, we argue that line-of-sight velocities of the young LMC members indicate that they have not traveled far during their lifetimes, and their current locations are representative of their birthplace. This points to *in situ* formation rather than being runaways from star-forming regions and stellar associations in the inner LMC. Moreover, stars #405 and #406 being so close to one another further argues against the likelihood of a runaway mechanism, since one would assume random directions for the ejecting stars.

Our findings are rather unexpected, since they point to star formation in the far outskirts of the LMC where gas density is currently low, $N_{HI} < 10^{19}$ cm $^{-2}$ (Fig. 7). Figure 5 clearly shows this as well; notice the small, inner LMC region occupied by emission nebulae and young stellar associations compared to the distribution of our stars. That the gaseous disk of the LMC is truncated when compared to the intermediate-age/old stellar disk is no longer a novelty since the work of Saha et al. (2010). Various theoretical models (see Hammer et al. 2015, and references therein) attribute this morphology primarily to truncation caused by ram pressure exerted by the Galactic hot halo gas. Traditional star-formation studies of the LMC disk, based on color-magnitude diagrams, indicate that the young star-forming epoch continues to the present time only in the inner $\sim 5^\circ$ of the disk (Meschin et al. 2014).

Whence these ~ 20 – 50 Myr stars in the far outskirts? One intriguing clue as to a possible origin is their half-ring spatial distribution, which was shown in Sec. 4.3 to be unlikely a mere random configuration. If these are, in fact, in the form of a circular ring in the plane of the LMC disk, it suggests an interesting possible formation scenario.

N-body/SPH simulations of collisions between a barred disk galaxy and a small (20% mass) satellite (Berentzen et al. 2003) show that an off-center collision produces expanding ring structures, off-center bars, and other asymmetries in the stars and gas. Typically, the impact produces a density wave in the host’s disk, which first becomes apparent in the gas. If the impact is off center, the symmetry of the gaseous ring is broken when it encounters spiral arms. In our case, the SMC had a recent collision with the LMC’s disk. The particulars of this collision — impact parameter and angle — will dictate the morphology of the outskirts of the LMC’s disk (see e.g., Besla et al. 2016, and references therein). It is thus conceivable that the formation of our five young stars which appear in a ring-like configuration was triggered by the recent collision between the SMC and the LMC’s disk. At the time the Mackey et al. (2016) study was completed, the DES did not cover the eastern portion of the outskirts of the LMC where our stars #307 and #390 lie; it

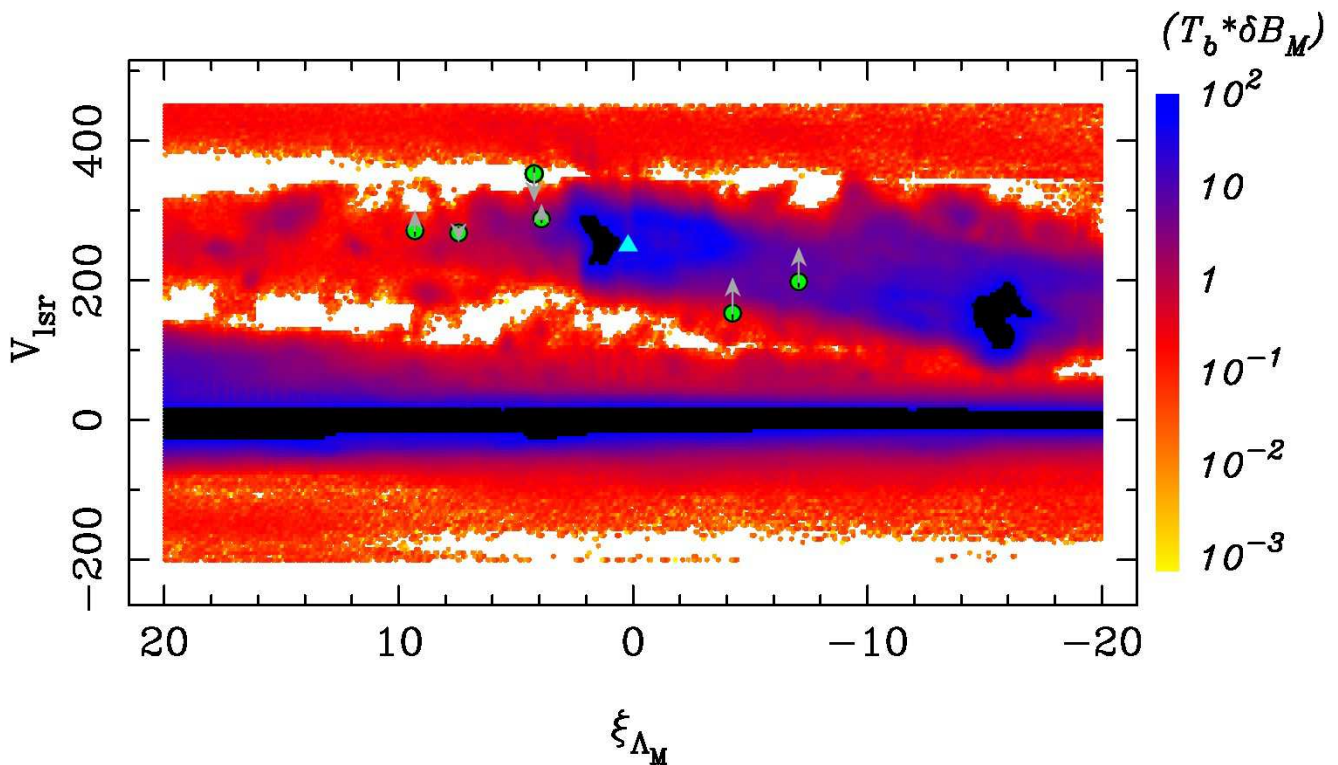


Figure 8. V_{1sr} as a function of ξ_{LM} along the LMC’s orbit. The color scale shows the temperature brightness integrated along η_{BM} for the range -30° to 30° . Black regions indicate values larger than 10^2 K deg, while white regions indicate values less than 10^{-3} K deg. Green symbols show our young LMC members. The LMC’s center is represented with a triangle. The arrows indicate the difference in velocity between our measurements and the predictions of a model of the LMC disk rotation, at each star’s position.

would be very informative to have that area covered by deep, contiguous photometric surveys.

The impact parameter of the collision between the SMC and the LMC disk appears to be moderate to small. Based on a simple orbit integration CD12 find an impact parameter of ~ 12 kpc as an upper limit, and an impact angle of $\sim 35^\circ$ (where 0° is coplanar). From dynamical models of the LMC-SMC interaction, Besla et al. (2016) find the impact parameter to be < 10 kpc in order to reproduce the arcs found in their study, while Besla et al. (2012) find it to be $2-5$ kpc in order to warp the bar out of the LMC disk plane. The center of our half-ring structure can be conjectured as the location of the impact between the SMC and LMC’s disk (see e.g., Mapelli & Mayer 2012). In Section 4.3 we determine the physical distance between the LMC’s center and that of the five-star ring to be 2.6 ± 0.3 kpc, a value that is toward the low end of the estimated impact parameter from models of the interaction. The uncertainty in this value is derived from δr (see Section 4.3), i.e., it is based on the fit of the five LMC stars. Nevertheless, our observations bring to light an as yet unknown aspect of the LMC-SMC interaction: the formation of young stars in a half-ring configuration in the outskirts of LMC’s disk. These observations should be useful in constraining the geometry of the collision from a totally new viewpoint, as well as provoking models of star formation in low gas environments.

5 SUMMARY

We have measured radial velocities and stellar parameters for thirty-one stars from the CD12 sample, candidates for being young OB stars in the periphery of the LMC; specifically between 6° and 33° from the LMC’s center. Twenty-one of our targets are foreground subdwarfs or white dwarfs, and one is an object of uncertain classification, likely a post-HB star. The remaining nine targets are young, hot, MS stars, whose distances and ages are determined in our study. We find that three of them are foreground to the LMC, probably runaway stars from the Galactic disk, while six of our targets are recently-formed stars at the distance of the LMC. The youngest of these (11 Myr) is a member of a known stellar association, ICA76, located in the Bridge. The remaining five stars span a narrow age range, between 18 and 45 Myr. These five MS objects are located between $\sim 8^\circ$ and 13° from LMC’s center in regions of low H I density, and appear to have formed in isolation. Their radial velocities follow the H I gas motions in the Magellanic system, and are not too deviant from the predictions of an LMC disk model. Specifically, velocity differences with the model are on average 36 km s^{-1} , which imply a travel distance of at most 1 kpc ($\sim 1^\circ$ at the LMC’s distance) during their lifetime. We argue that these stars were formed *in situ* rather than being runaways from the inner disk of the LMC. Their spatial configuration appears ring-like, and is suggestive of a formation process triggered by the recent collision of the SMC with the LMC disk at a modest, 4-kpc impact parameter. Highly accurate trigonometric parallaxes and absolute proper mo-

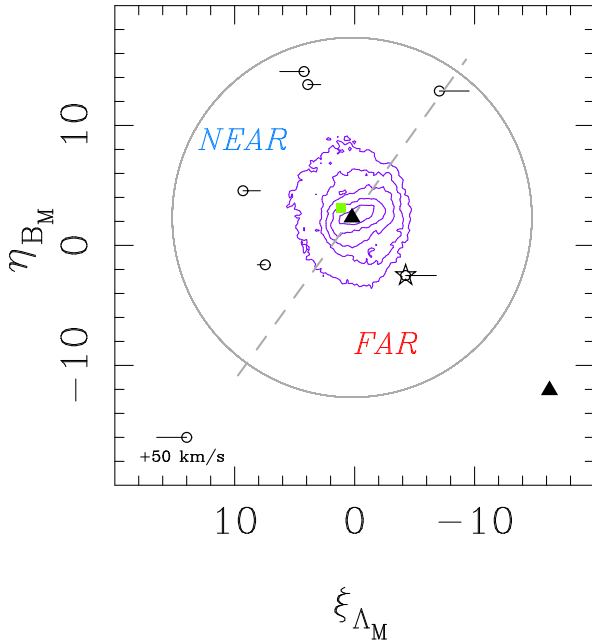


Figure 9. The sky distribution of the six young LMC members with V_{lsr} differences (observed - model) shown as horizontal vectors. A vector of $+50 \text{ km s}^{-1}$ is shown in the bottom left corner for scale. Triangles mark the centers of the LMC and SMC. The star symbol shows the stellar member of ICA76. The green square indicates the location of 30 Doradus. Contours represent isodensity curves of M giants in the LMC selected from 2MASS. The line of nodes of the disk is shown with a dashed line, with the near and far sides of the disk labeled. The circle highlights a radius of 15° from LMC's center.

tions for these young stars, as is expected within the next few years from the Gaia mission, should readily confirm or refute this possible explanation. Regardless of their apparent geometric configuration, these newly identified LMC members represent a feature that, unlike previously discovered structures in the periphery of the disk, is traced by young stars.

ACKNOWLEDGEMENTS

This study was based on observations gathered at the 6.5 meter Magellan Telescopes located at Las Campanas Observatory, Chile (program ID CHILE-2015A-029). C.M.B. acknowledges support from FONDECYT through regular project 1150060. R.A.M. acknowledges support from the Chilean Centro de Excelencia en Astrofísica y Tecnologías Afines (CATA) BASAL PFB/06 and from the Project IC120009 Millennium Institute of Astrophysics (MAS) of the Iniciativa Científica Milenio del Ministerio de Economía, Fomento y Turismo de Chile. L.Z. acknowledges supports from the Chinese Academy of Sciences (CAS) through a CAS-CONICYT Postdoctoral Fellowship and partial supports from NSFC grants 11303037 and 11390371. V.K. acknowledges the financial support by the RFBR grant 15-02-06204-a.

REFERENCES

- Bagheri G., Cioni M.-R. L., Napiwotzki R., 2013, *A&A*, **551**, A78
 Battinelli P., Demers S., 1992, *AJ*, **104**, 1458
 Belokurov V., Koposov S. E., 2016, *MNRAS*, **456**, 602
 Berentzen I., Athanassoula E., Heller C. H., Fricke K. J., 2003, *MNRAS*, **341**, 343
 Bergeron P., Saffer R. A., Liebert J., 1992, *ApJ*, **394**, 228
 Besla G., Kallivayalil N., Hernquist L., van der Marel R. P., Cox T. J., Kereš D., 2012, *MNRAS*, **421**, 2109
 Besla G., Martínez-Delgado D., van der Marel R. P., Beletsky Y., Seibert M., Schlafly E. F., Grebel E. K., Neyer F., 2016, *ApJ*, **825**, 20
 Bianchi L., Efremova B., Herald J., Girardi L., Zobot A., Marigo P., Martin C., 2011, *MNRAS*, **411**, 2770
 Bica E., Bonatto C., Dutra C. M., Santos J. F. C., 2008, *MNRAS*, **389**, 678
 Bonifacio P., Monai S., Beers T. C., 2000, *AJ*, **120**, 2065
 Bressan A., Marigo P., Girardi L., Salasnich B., Dal Cero C., Rubele S., Nanni A., 2012, *MNRAS*, **427**, 127
 Casetti-Dinescu D. I., Vieira K., Girard T. M., van Altena W. F., 2012, *ApJ*, **753**, 123
 Casetti-Dinescu D. I., Moni Bidin C., Girard T. M., Méndez R. A., Vieira K., Korchagin V. I., van Altena W. F., 2014, *ApJ*, **784**, L37
 Chubak C., Marcy G., Fischer D. A., Howard A. W., Isaacson H., Johnson J. A., Wright J. T., 2012, ArXiv:1207.6212,
 D'Onghia E., Fox A. J., 2015, ArXiv:1511.05853,
 Demers S., Battinelli P., 1998, *AJ*, **115**, 154
 Edelmann H., Heber U., Hagen H.-J., Lemke M., Dreizler S., Napiwotzki R., Engels D., 2003, *A&A*, **400**, 939
 Freedman W. L., et al., 2001, *ApJ*, **553**, 47
 Gardiner L. T., Noguchi M., 1996, *MNRAS*, **278**, 191
 Geier S., Heber U., 2012, *A&A*, **543**, A149
 Girard T. M., et al., 2011, *AJ*, **142**, 15
 Hammer F., Yang Y. B., Flores H., Puech M., Fouquet S., 2015, *ApJ*, **813**, 110
 Han Z., 2008, *A&A*, **484**, L31
 Harris J., 2007, *ApJ*, **658**, 345
 Heber U., 1986, *A&A*, **155**, 33
 Henden A. A., Levine S. E., Terrell D., Smith T. C., Welch D. L., 2011, in American Astronomical Society Meeting Abstracts #218. p. 126.01
 Hindman J. V., Kerr F. J., McGee R. X., 1963, *Australian Journal of Physics*, **16**, 570
 Horne K., 1986, *PASP*, **98**, 609
 Irwin M. J., Demers S., Kunkel W. E., 1990, *AJ*, **99**, 191
 James P. A., Ivory C. F., 2011, *MNRAS*, **411**, 495
 Kalberla P. M. W., Haud U., 2015, *A&A*, **578**, A78
 Kerr F. J., 1957, *AJ*, **62**, 93
 Kurucz R., 1993, ATLAS9 Stellar Atmosphere Programs and 2 km/s grid. Kurucz CD-ROM No. 13. Cambridge, Mass.: Smithsonian Astrophysical Observatory, 1993., **13**
 Latham D. W., Stefanik R. P., Torres G., Davis R. J., Mazeh T., Carney B. W., Laird J. B., Morse J. A., 2002, *AJ*, **124**, 1144
 Liu L., Gerke B. F., Wechsler R. H., Behroozi P. S., Busha M. T., 2011, *ApJ*, **733**, 62
 Mackey A. D., Koposov S. E., Erkal D., Belokurov V., Da Costa G. S., Gómez F. A., 2016, *MNRAS*, **459**, 239
 Mapelli M., Mayer L., 2012, *MNRAS*, **420**, 1158
 Mason B. D., Gies D. R., Hartkopf W. I., Bagnuolo Jr. W. G., ten Brummelaar T., McAlister H. A., 1998, *AJ*, **115**, 821
 Mathewson D. S., Cleary M. N., Murray J. D., 1974, *ApJ*, **190**, 291
 Maxted P. F. L., Heber U., Marsh T. R., North R. C., 2001, *MNRAS*, **326**, 1391
 McMonigal B., et al., 2014, *MNRAS*, **444**, 3139

- Meschin I., Gallart C., Aparicio A., Hidalgo S. L., Monelli M., Stetson P. B., Carrera R., 2014, *MNRAS*, **438**, 1067
- Moehler S., Sweigart A. V., Catelan M., 1999, *A&A*, **351**, 519
- Moehler S., Sweigart A. V., Landsman W. B., Heber U., 2000, *A&A*, **360**, 120
- Moehler S., Sweigart A. V., Landsman W. B., Hammer N. J., Dreizler S., 2004, *A&A*, **415**, 313
- Moni Bidin C., Moehler S., Piotto G., Recio-Blanco A., Momany Y., Méndez R. A., 2006, *A&A*, **451**, 499
- Moni Bidin C., Catelan M., Altmann M., 2008, *A&A*, **480**, L1
- Moni Bidin C., Moehler S., Piotto G., Momany Y., Recio-Blanco A., 2009, *A&A*, **498**, 737
- Moni Bidin C., Villanova S., Piotto G., Momany Y., 2011, *A&A*, **528**, A127
- Moni Bidin C., Casetti-Dinescu D. I., Méndez R. A., Girard T. M., Vieira K., Korchagin V. I., van Altena W. F., 2015, in Points S., Kunder A., eds, ASP Conference Series Vol. 491, Fifty Years of Wide Field Studies in the Southern Hemisphere: Resolved Stellar Populations of the Galactic Bulge and Magellanic Clouds. p. 272
- Morse J. A., Mathieu R. D., Levine S. E., 1991, *AJ*, **101**, 1495
- Muñoz R. R., et al., 2006, *ApJ*, **649**, 201
- Munari U., Sordo R., Castelli F., Zwitter T., 2005, *A&A*, **442**, 1127
- Murray C. E., et al., 2015, *ApJ*, **808**, 41
- Napiwotzki R., 1997, *A&A*, **322**, 256
- Napiwotzki R., Green P. J., Saffer R. A., 1999, *ApJ*, **517**, 399
- Nidever D. L., Majewski S. R., Butler Burton W., Nigra L., 2010, *ApJ*, **723**, 1618
- Noël N. E. D., Conn B. C., Read J. I., Carrera R., Dolphin A., Rix H.-W., 2015, *MNRAS*, **452**, 4222
- Olsen K. A. G., Zaritsky D., Blum R. D., Boyer M. L., Gordon K. D., 2011, *ApJ*, **737**, 29
- Piatti A. E., 2016, *MNRAS*, **459**, L61
- Pieres A., et al., 2016, *MNRAS*, **461**, 519
- Saffer R. A., Bergeron P., Koester D., Liebert J., 1994, *ApJ*, **432**, 351
- Saha A., Olszewski E. W., 2015, in Points S., Kunder A., eds, Astronomical Society of the Pacific Conference Series Vol. 491, Fifty Years of Wide Field Studies in the Southern Hemisphere: Resolved Stellar Populations of the Galactic Bulge and Magellanic Clouds. p. 317
- Saha A., et al., 2010, *AJ*, **140**, 1719
- Salgado C., Moni Bidin C., Villanova S., Geisler D., Catelan M., 2013, *A&A*, **559**, A101
- Sana H., et al., 2012, *Science*, **337**, 444
- Schlegel D. J., Finkbeiner D. P., Davis M., 1998, *ApJ*, **500**, 525
- Simkin S. M., 1974, *A&A*, **31**, 129
- Skowron J., et al., 2016, *ApJ*, **820**, 4
- Skrutskie M. F., et al., 2006, *AJ*, **131**, 1163
- Suntzeff N. B., Schommer R. A., Olszewski E. W., Walker A. R., 1992, *AJ*, **104**, 1743
- Tonry J., Davis M., 1979, *AJ*, **84**, 1511
- de la Fuente Marcos R., de la Fuente Marcos C., Moni Bidin C., Ortolani S., Carraro G., 2015, *A&A*, **581**, A13
- van der Marel R. P., Alves D. R., Hardy E., Suntzeff N. B., 2002, *AJ*, **124**, 2639

This paper has been typeset from a $\text{\TeX}/\text{\LaTeX}$ file prepared by the author.